Nonlinear Force-Free Magnetic Field Modeling of the Solar Corona: <u>A Critical Assessment</u>

Marc DeRosa (LMSAL)
on behalf of the *NLFFF working group**

Hinode 2 Science Meeting ~ Boulder, CO ~ Sept. 30, 2008

**Karel Schrijver, Graham Barnes, KD Leka, Bruce Lites, Markus Aschwanden, Jim McTiernan, Stéphane Régnier, Julia Thalmann, Gherardo Valori, Mike Wheatland, Thomas Wiegelmann, Mark Cheung, Paul Conlon, Marcel Fuhrmann, Bernd Inhester, Tilaye Tadesse*

Rationale

- Understanding the dynamical structure and evolution of the solar corona requires a *quantitative understanding of the coronal magnetic field and its currents*.
- *Nonlinear force-free fields (NLFFFs) provide a useful model*. The magnetic field is determined inside a computational volume, subject to $(\nabla \times \boldsymbol{B}) \times \boldsymbol{B} = 0$, or $\boldsymbol{J} = \alpha\, \boldsymbol{B}$.
- The scalar α is invariant along fieldlines of $\boldsymbol{B}$.
- In general, α varies spatially, making the problem of solving for $\boldsymbol{B}$ nonlinear.

Algorithms

- Three popular algorithms:
  - *Optimization* [minimize a metric containing $(\nabla \times \boldsymbol{B}) \times \boldsymbol{B}$ and $\nabla \cdot \boldsymbol{B}$]
  - *Current-field iteration* [initialize field, apply currents based on surface α, recompute field, iterate…, stop when a fixed point is (hopefully) reached]
  - *Magneto-frictional* [solve a MHD-like system of equations, including an ad-hoc friction term that drives the system toward a force-free state]

Previously…

- We performed 14 extrapolations for each of two Hinode/SOT-SP vector magnetogram scans bracketing the X flare that occurred on 13 Dec 2006 in AR 10930.

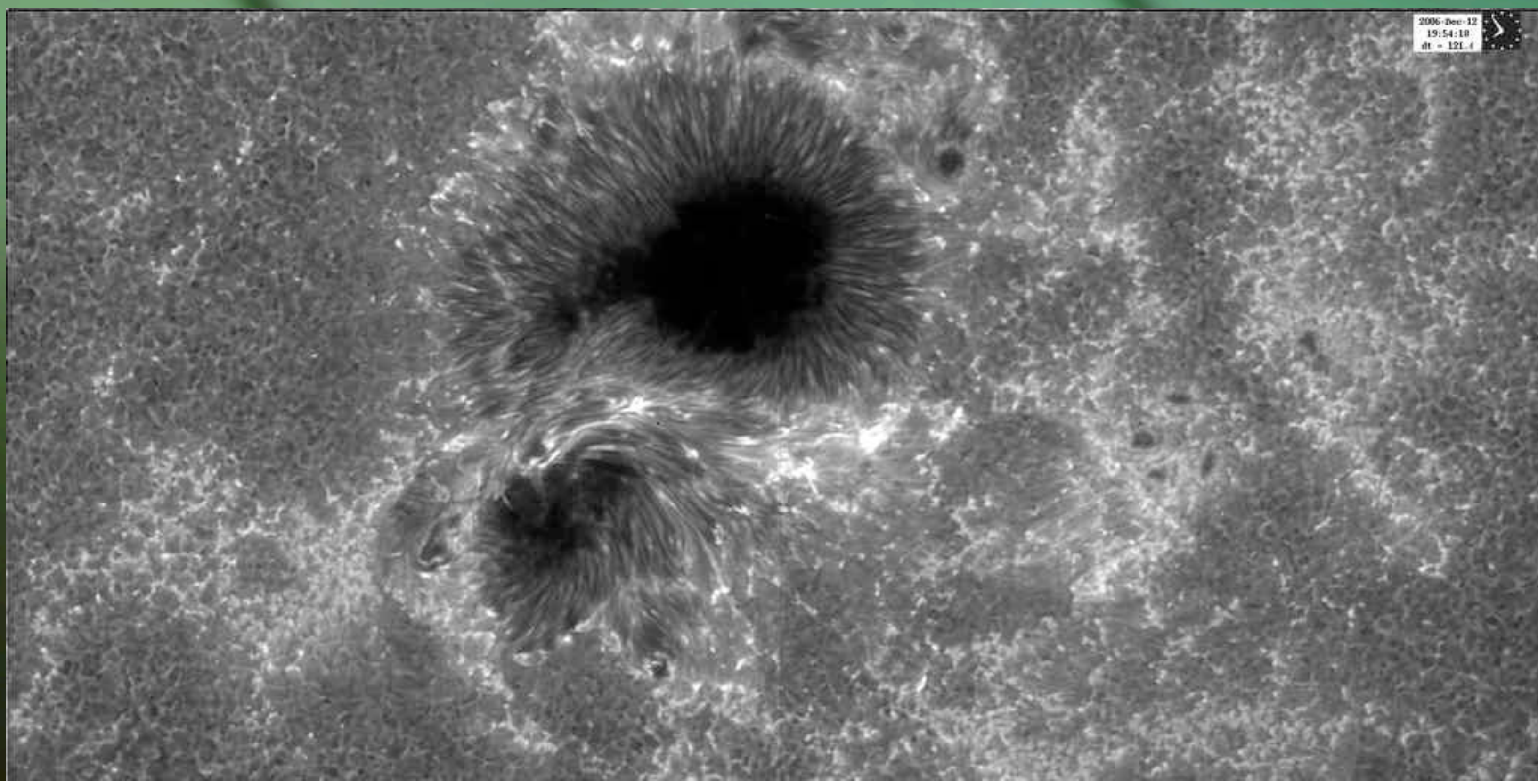

Ca II H from Hinode/SOT-BFI

Hinode/XRT overlay - preflare

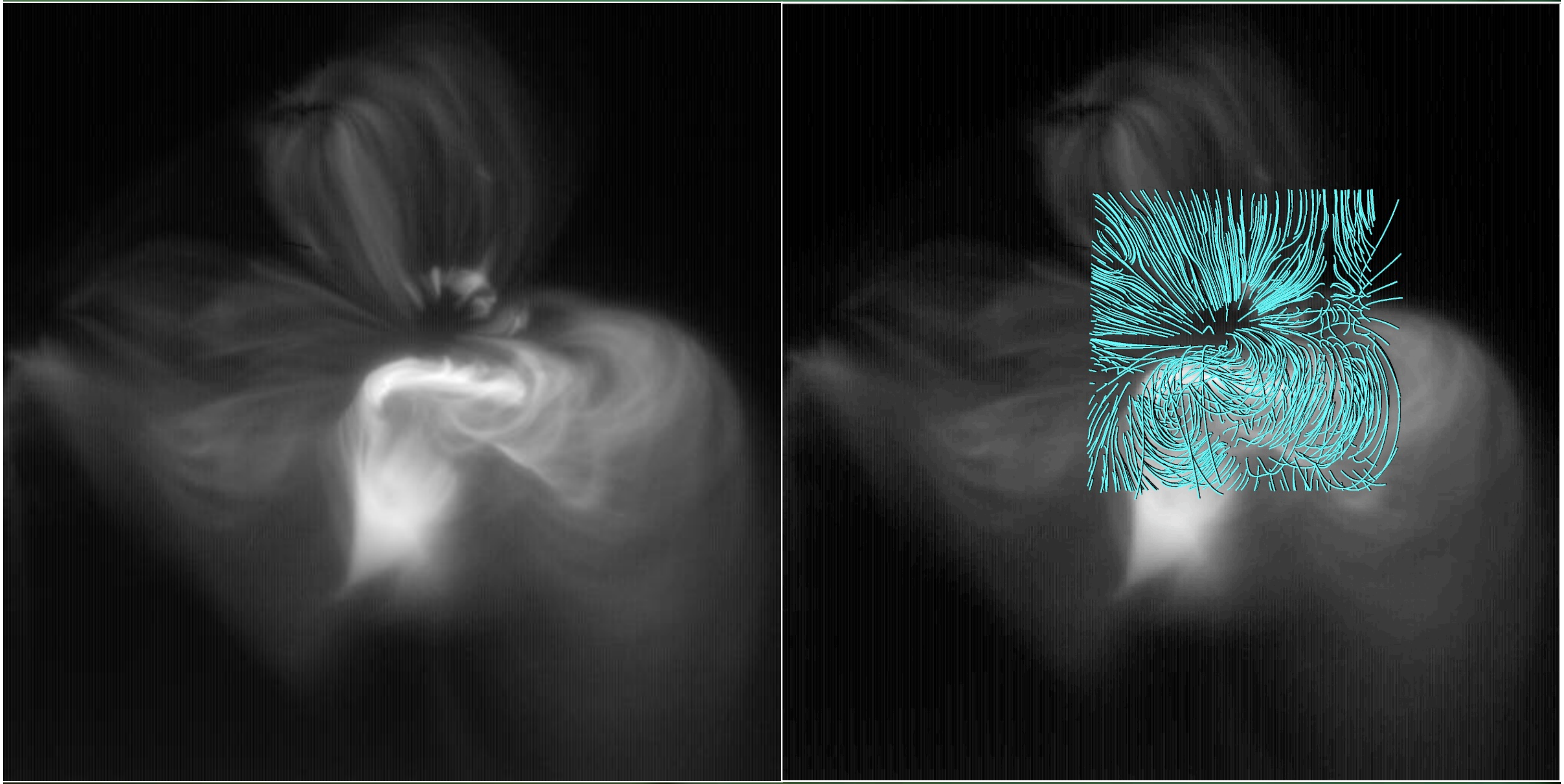

fieldlines contained within a 320×320×128-pixel volume

2006.12.12_2030

Volume renderings of current density

pre-flare

post-flare

difference in free energy = 3×10^{32} erg

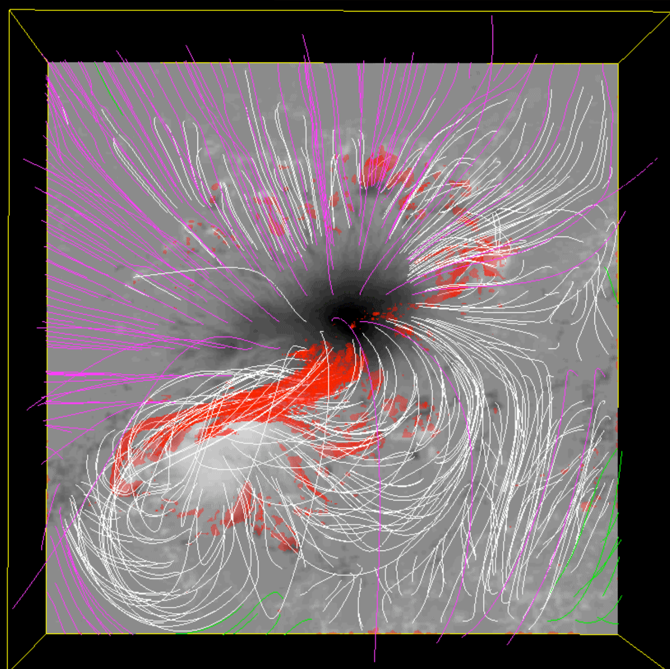

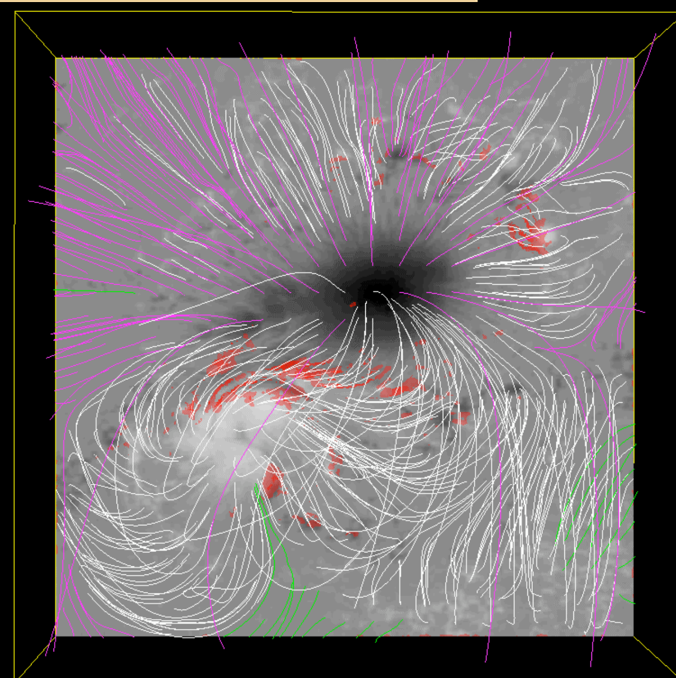

isosurface of |***J***| shown in red

$E/E_{pot}=1.32$

$E/E_{pot}=1.14$

Free energies for AR 10930

pre-flare

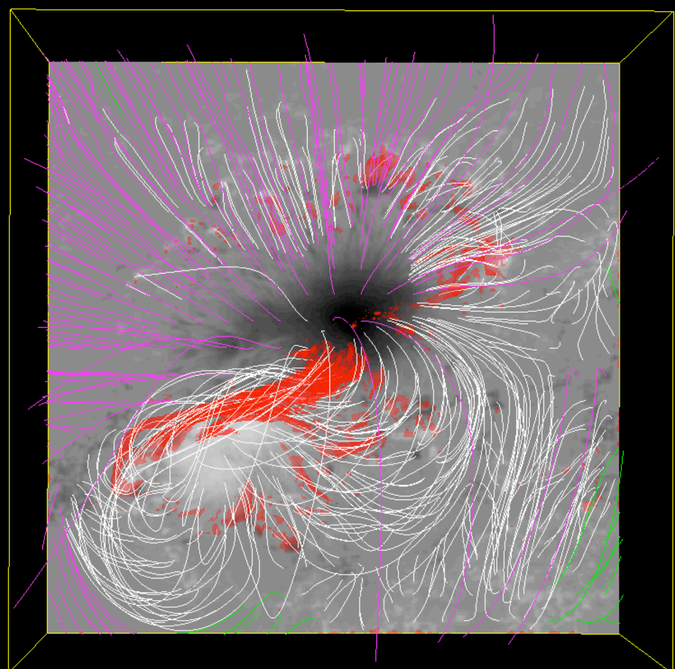

isosurface of |*J*| shown in red

E/E_{pot}=1.32

Model	pre-flare E/E_{pot}
Wh^{+}_{pp}	1.32
Wh^{+}_{np}	1.10
Wie_{wp}	1.09
Val_{pp}	1.10
Wh^{0}_{pp}	1.04
Wie_{ns}	1.04
Val_{np}	0.88
Wie_{np}	0.95
Wie_{pp}	1.05
McT_{pp}	1.01
Wh^{0}_{np}	1.03
Wh^{-}_{np}	1.04
Wh^{-}_{pp}	1.05
McT_{np}	0.95
Potential	1.00

From Table 1 of Schrijver et al. (2008)

Free energies for AR 10930

pre-flare

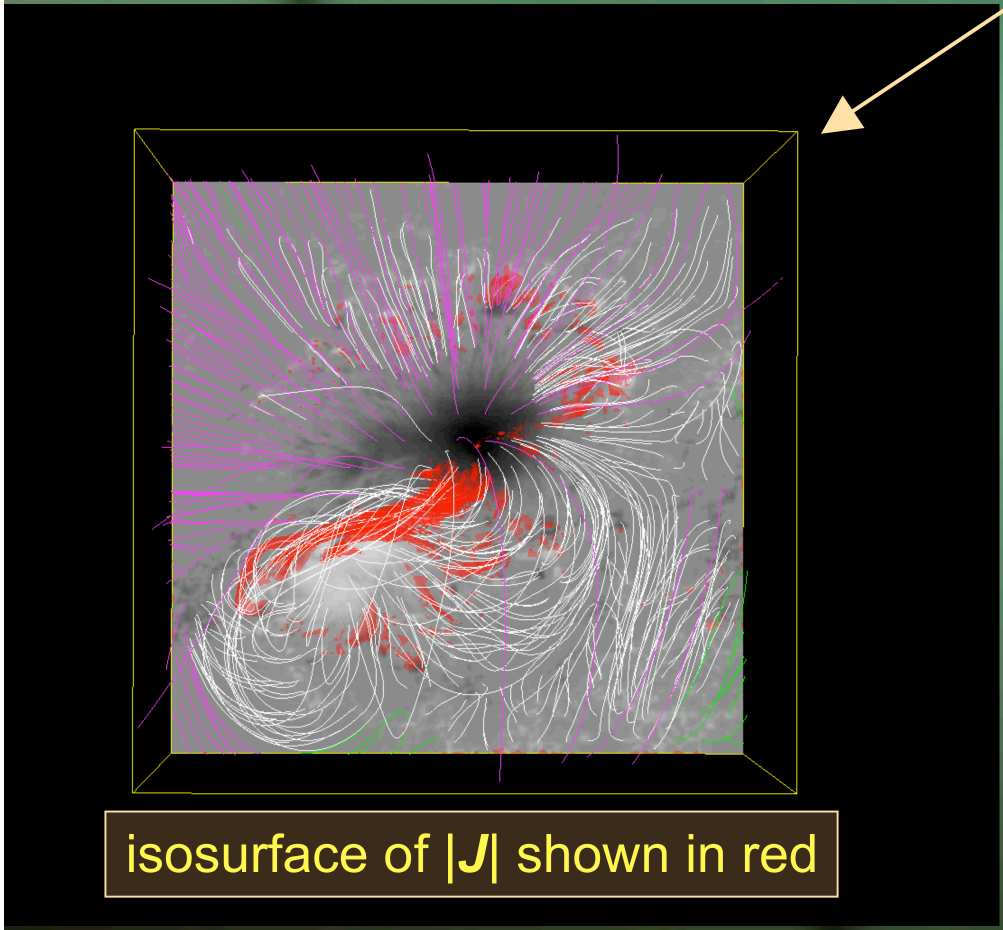

E/E_{pot}=1.32

Model	pre-flare E/E_{pot}
Wh^{+}_{pp}	1.32
Wh^{+}_{np}	1.10
Wie_{wp}	1.09
Val_{pp}	1.10
Wh^{0}_{pp}	1.04
Wie_{ns}	1.04
Val_{np}	0.88
Wie_{np}	0.95
Wie_{pp}	1.05
McT_{pp}	1.01
Wh^{0}_{np}	1.03
Wh^{-}_{np}	1.04
Wh^{-}_{pp}	1.05
McT_{np}	0.95
Potential	1.00

From Table 1 of Schrijver et al. (2008)

Table of metrics for AR 10930

Metrics for the Field Extrapolations, in Order of Quality Q Based on the Visual Correspondence to the Coronal Preflare Image

		Preflare: 2006 Dec. 12			Postflare: 2006 Dec. 13		
Model[1]	Q_m[2]	$E/E_{p,\mathrm{pre}}$[3]	CW $\sin\theta$[4]	$\langle\lvert f_i\rvert\rangle \times 10^8$[5]	$E/E_{p,\mathrm{pre}}$	CW $\sin\theta$	$\langle\lvert f_i\rvert\rangle \times 10^8$
$\mathrm{Wh}^{+}_{\mathrm{pp}}$	5	1.32	0.24	3.6	1.19	0.18	2.0
$\mathrm{Wh}^{+}_{\mathrm{np}}$	3	1.10	0.27	3.9	1.23	0.27	4.6
$\mathrm{Wie}_{\mathrm{wp}}$	3	1.09	0.35	19	1.18	0.32	13
$\mathrm{Val}_{\mathrm{pp}}$	3	1.10	0.28	230	1.27	0.31	190
$\mathrm{Wh}^{0}_{\mathrm{pp}}$	2	1.04	0.28	3.0	1.53	0.27	3.7
$\mathrm{Wie}_{\mathrm{ns}}$	2	1.04	0.43	22	1.13	0.39	30
$\mathrm{Val}_{\mathrm{np}}$	2	0.88	0.29	220	0.99	0.34	210
$\mathrm{Wie}_{\mathrm{np}}$	1	0.95	0.43	24	1.04	0.39	27
$\mathrm{Wie}_{\mathrm{pp}}$	0	1.05	0.44	18	1.15	0.39	21
$\mathrm{McT}_{\mathrm{pp}}$	0	1.01	0.61	29	1.07	0.59	25
$\mathrm{Wh}^{0}_{\mathrm{np}}$	−1	1.03	0.27	2.5	1.12	0.23	2.6
$\mathrm{Wh}^{-}_{\mathrm{np}}$	−1	1.04	0.25	2.9	1.11	0.24	2.9
$\mathrm{Wh}^{-}_{\mathrm{pp}}$	−1	1.05	0.27	3.2	1.16	0.19	2.2
$\mathrm{McT}_{\mathrm{np}}$	−2	0.95	0.64	26	1.00	0.61	24
Potential	−3	1	...	0.8	1.04	...	0.8

[1] Models: Wh: Wheatland; Wie: Wiegelmann; Val: Valori; McT: McTiernan; +, −, 0: based on positive or negative B_z, or both, respectively; np: no preprocessing; ns: preprocessed without smoothing; pp: preprocessing including smoothing; wp: Wiegelmann's preprocessing and smoothing.

[2] Quality of fit by visual inspection for five features: a good or poor correspondence for each feature adds +1 or −1, respectively, to the total value; an ambiguous correspondence adds 0.

[3] Energy, relative to the energy in the preflare potential field model.

[4] Current-weighted value of $\sin\theta$, where θ is the angle between the electrical current and the magnetic field in the model solution.

[5] The unsigned mean over all pixels i in the comparison volume of the absolute fractional flux change $\lvert f_i\rvert = \lvert(\nabla \cdot \boldsymbol{B})_i\rvert/(6\lvert\boldsymbol{B}\rvert_i/\Delta x)$, where Δx is the grid spacing (cf. Wheatland et al. 2000).

Schrijver et al. (2008)

Table of metrics for AR 10930

Metrics for the Field Extrapolations, in Order of Quality Q Based on the Visual Correspondence to the Coronal Preflare Image

		Preflare: 2006 Dec. 12			Postflare: 2006 Dec. 13		
Model[1]	Q_m[2]	$E/E_{p,\mathrm{pre}}$[3]	CW $\sin\theta$[4]	$\langle\lvert f_i\rvert\rangle \times 10^8$[5]	$E/E_{p,\mathrm{pre}}$	CW $\sin\theta$	$\langle\lvert f_i\rvert\rangle \times 10^8$
$\mathrm{Wh}^{+}_{\mathrm{pp}}$	5	1.32	0.24	3.6	1.19	0.18	2.0
$\mathrm{Wh}^{+}_{\mathrm{np}}$	3	1.10	0.27	3.9	1.23	0.27	4.6
$\mathrm{Wie}_{\mathrm{wp}}$	3	1.09	0.35	19	1.18	0.32	13
$\mathrm{Val}_{\mathrm{pp}}$	3	1.10	0.28	230	1.27	0.31	190
$\mathrm{Wh}^{0}_{\mathrm{pp}}$	2	1.04	0.28	3.0	1.53	0.27	3.7
$\mathrm{Wie}_{\mathrm{ns}}$	2	1.04	0.43	22	1.13	0.39	30
$\mathrm{Val}_{\mathrm{np}}$	2	0.88	0.29	220	0.99	0.34	210
$\mathrm{Wie}_{\mathrm{np}}$	1	0.95	0.43	24	1.04	0.39	27
$\mathrm{Wie}_{\mathrm{pp}}$	0	1.05	0.44	18	1.15	0.39	21
$\mathrm{McT}_{\mathrm{pp}}$	0	1.01	0.61	29	1.07	0.59	25
$\mathrm{Wh}^{0}_{\mathrm{np}}$	−1	1.03	0.27	2.5	1.12	0.23	2.6
$\mathrm{Wh}^{-}_{\mathrm{np}}$	−1	1.04	0.25	2.9	1.11	0.24	2.9
$\mathrm{Wh}^{-}_{\mathrm{pp}}$	−1	1.05	0.27	3.2	1.16	0.19	2.2
$\mathrm{McT}_{\mathrm{np}}$	−2	0.95	0.64	26	1.00	0.61	24
Potential	−3	1	...	0.8	1.04	...	0.8

[1] Models: Wh: Wheatland; Wie: Wiegelmann; Val: Valori; McT: McTiernan; +, −, 0: based on positive or negative B_z, or both, respectively; np: no preprocessing; ns: preprocessed without smoothing; pp: preprocessing including smoothing; wp: Wiegelmann's preprocessing and smoothing.

[2] Quality of fit by visual inspection for five features: a good or poor correspondence for each feature adds +1 or −1, respectively, to the total value; an ambiguous correspondence adds 0.

[3] Energy, relative to the energy in the preflare potential field model.

[4] Current-weighted value of $\sin\theta$, where θ is the angle between the electrical current and the magnetic field in the model solution.

[5] The unsigned mean over all pixels i in the comparison volume of the absolute fractional flux change $\lvert f_i\rvert = \lvert(\nabla\cdot\boldsymbol{B})_i\rvert/(6\lvert\boldsymbol{B}\rvert_i/\Delta x)$, where Δx is the grid spacing (cf. Wheatland et al. 2000).

Schrijver et al. (2008)

Table of metrics for AR 10930

Metrics for the Field Extrapolations, in Order of Quality Q Based on the Visual Correspondence to the Coronal Preflare Image

		Preflare: 2006 Dec. 12			Postflare: 2006 Dec. 13		
Model[1]	Q_m[2]	$E/E_{p,\mathrm{pre}}$[3]	CW $\sin\theta$[4]	$\langle\lvert f_i\rvert\rangle \times 10^8$[5]	$E/E_{p,\mathrm{pre}}$	CW $\sin\theta$	$\langle\lvert f_i\rvert\rangle \times 10^8$
$\mathrm{Wh}^{+}_{\mathrm{pp}}$	5	1.32	0.24	3.6	1.19	0.18	2.0
$\mathrm{Wh}^{+}_{\mathrm{np}}$	3	1.10	0.27	3.9	1.23	0.27	4.6
$\mathrm{Wie}_{\mathrm{wp}}$	3	1.09	0.35	19	1.18	0.32	13
$\mathrm{Val}_{\mathrm{pp}}$	3	1.10	0.28	230	1.27	0.31	190
$\mathrm{Wh}^{0}_{\mathrm{pp}}$	2	1.04	0.28	3.0	1.53	0.27	3.7
$\mathrm{Wie}_{\mathrm{ns}}$	2	1.04	0.43	22	1.13	0.39	30
$\mathrm{Val}_{\mathrm{np}}$	2	0.88	0.29	220	0.99	0.34	210
$\mathrm{Wie}_{\mathrm{np}}$	1	0.95	0.43	24	1.04	0.39	27
$\mathrm{Wie}_{\mathrm{pp}}$	0	1.05	0.44	18	1.15	0.39	21
$\mathrm{McT}_{\mathrm{pp}}$	0	1.01	0.61	29	1.07	0.59	25
$\mathrm{Wh}^{0}_{\mathrm{np}}$	−1	1.03	0.27	2.5	1.12	0.23	2.6
$\mathrm{Wh}^{-}_{\mathrm{np}}$	−1	1.04	0.25	2.9	1.11	0.24	2.9
$\mathrm{Wh}^{-}_{\mathrm{pp}}$	−1	1.05	0.27	3.2	1.16	0.19	2.2
$\mathrm{McT}_{\mathrm{np}}$	−2	0.95	0.64	26	1.00	0.61	24
Potential	−3	1	...	0.8	1.04	...	0.8

[1] Models: Wh: Wheatland; Wie: Wiegelmann; Val: Valori; McT: McTiernan; +, −, 0: based on positive or negative B_z, or both, respectively; np: no preprocessing; ns: preprocessed without smoothing; pp: preprocessing including smoothing; wp: Wiegelmann's preprocessing and smoothing.

[2] Quality of fit by visual inspection for five features: a good or poor correspondence for each feature adds +1 or −1, respectively, to the total value; an ambiguous correspondence adds 0.

[3] Energy, relative to the energy in the preflare potential field model.

[4] Current-weighted value of $\sin\theta$, where θ is the angle between the electrical current and the magnetic field in the model solution.

[5] The unsigned mean over all pixels i in the comparison volume of the absolute fractional flux change $\lvert f_i\rvert = \lvert(\nabla \cdot \boldsymbol{B})_i\rvert/(6\lvert\boldsymbol{B}\rvert_i/\Delta x)$, where Δx is the grid spacing (cf. Wheatland et al. 2000).

Schrijver et al. (2008)

Recap for AR 10930

- In the best-matching model for the 2006 Dec 13 flare, *free energy drops from 32% to 14% of potential energy, corresponding to a drop in free energy of 3×10^{32} erg.*
- Several issues/caveats:
  - *NLFFF calculations do not reach a consensus for this case*. A greater degree of robustness is desired before stronger conclusions can be drawn.
  - *EUV and x-ray coverage was not optimal for this region*, making it hard to determine best-fit model.
  - *Lower boundary did not fully contain both flare ribbons*, which may be associated with additional current systems used to power the eruption.

Now…

- We performed extrapolations based on Hinode/SOT-SP vector magnetogram scan of AR 10953 on 30 Apr 2007.

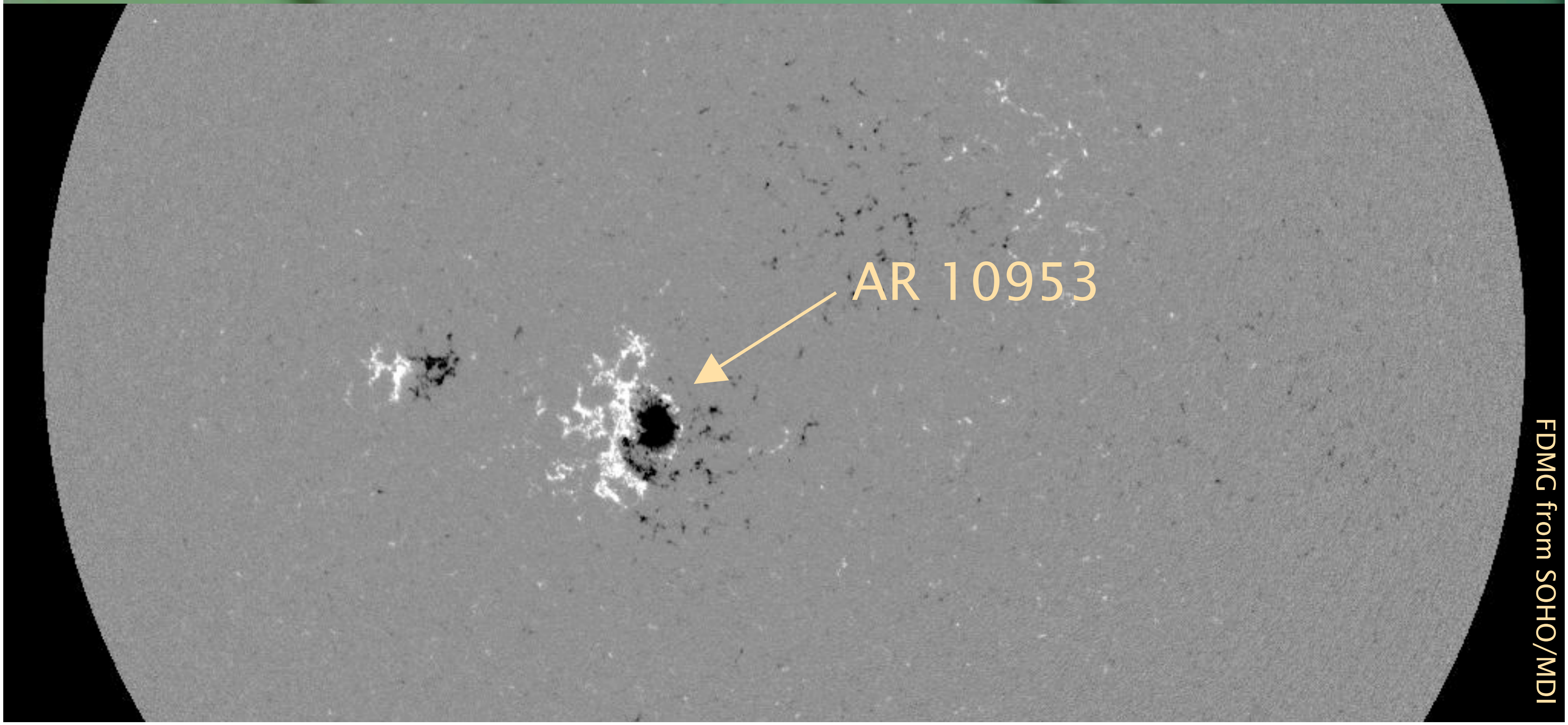

Now…

- We performed extrapolations based on Hinode/SOT-SP vector magnetogram scan of AR 10953 on 30 Apr 2007.

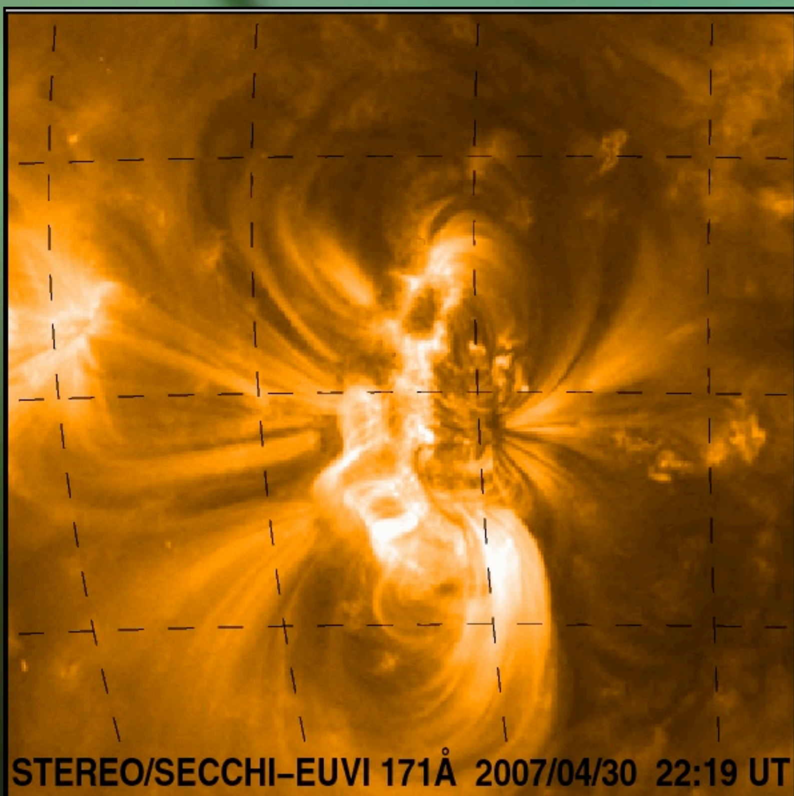

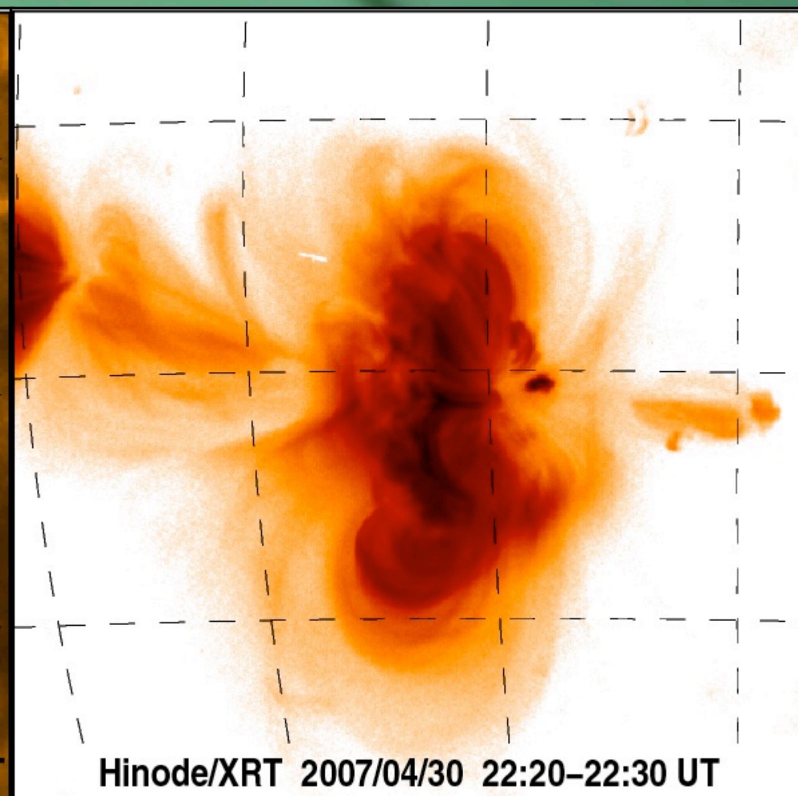

Now…

- We performed extrapolations based on Hinode/SOT-SP vector magnetogram scan of AR 10953 on 30 Apr 2007.

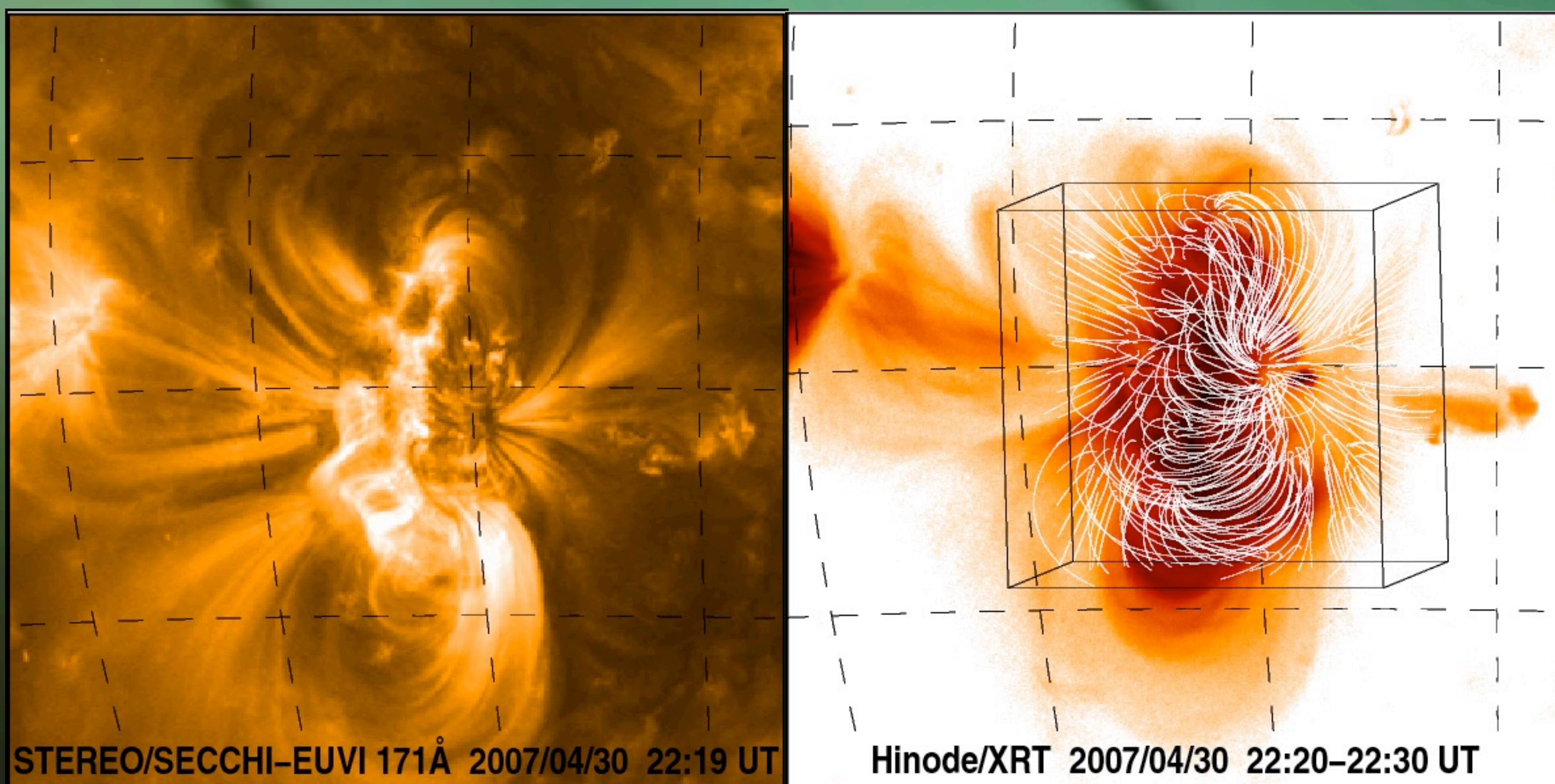

Comparison with STEREO

- We compared model fieldlines to three-dimensional loop trajectories determined using stereoscopy (applied to STEREO/SECCHI-EUVI).

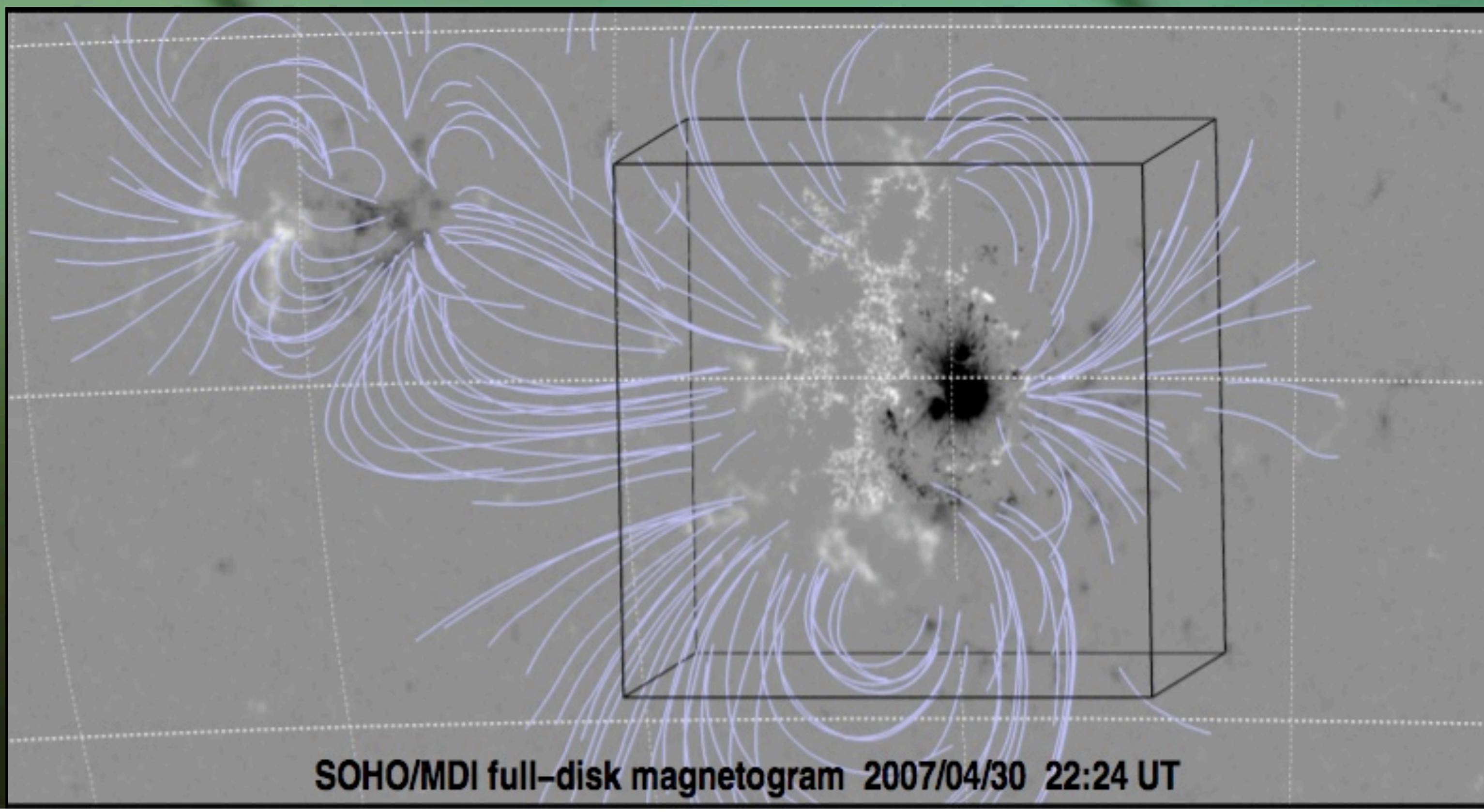

Comparison with STEREO

- We compared model fieldlines to three-dimensional loop trajectories determined using stereoscopy (applied to STEREO/SECCHI-EUVI).

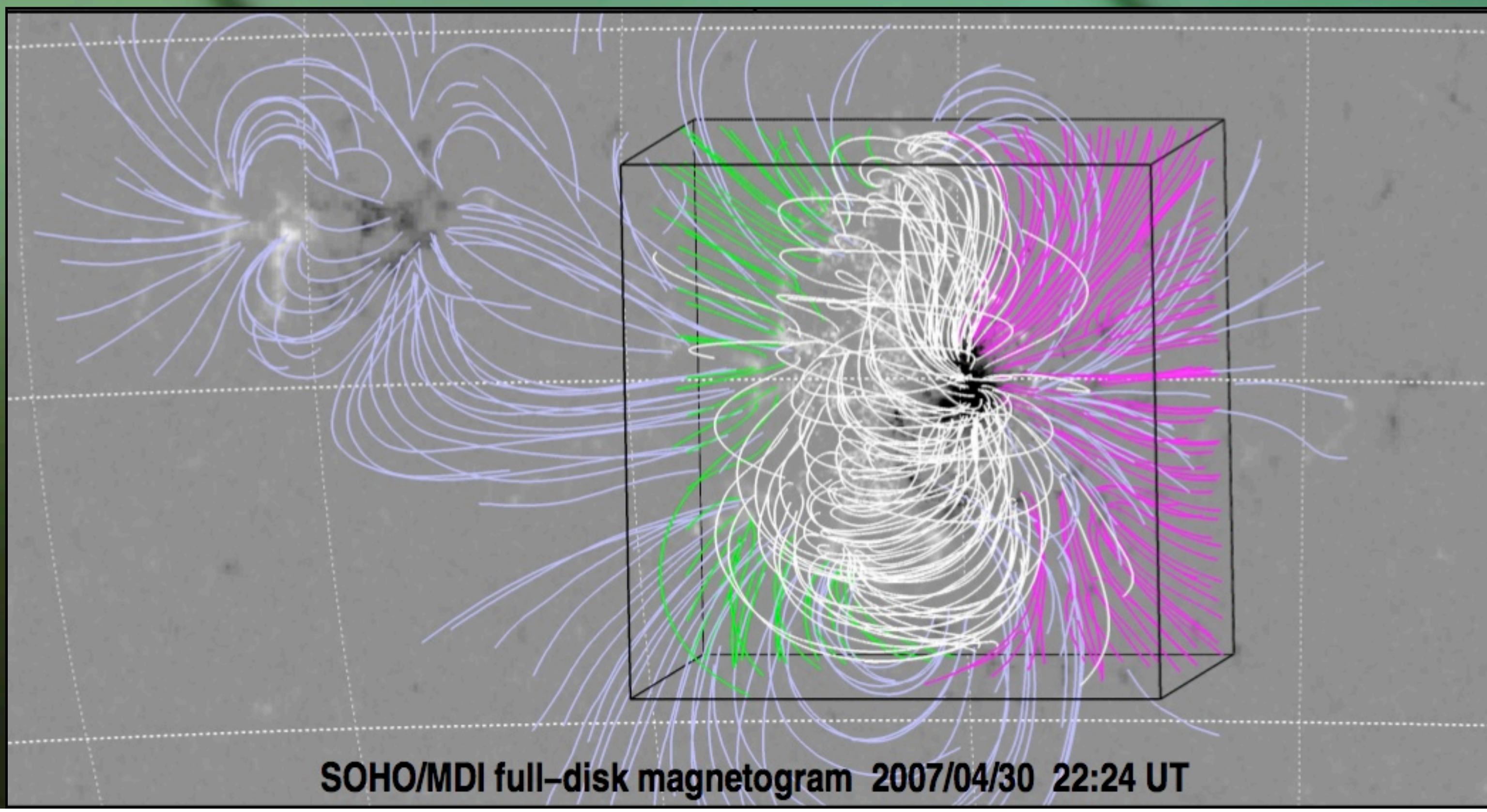

Comparison with STEREO

- We compared model fieldlines to three-dimensional loop trajectories determined using stereoscopy (applied to STEREO/SECCHI-EUVI).
- Alignment: $\phi < 5^\circ$ (yellow), $\phi > 45^\circ$ (red)

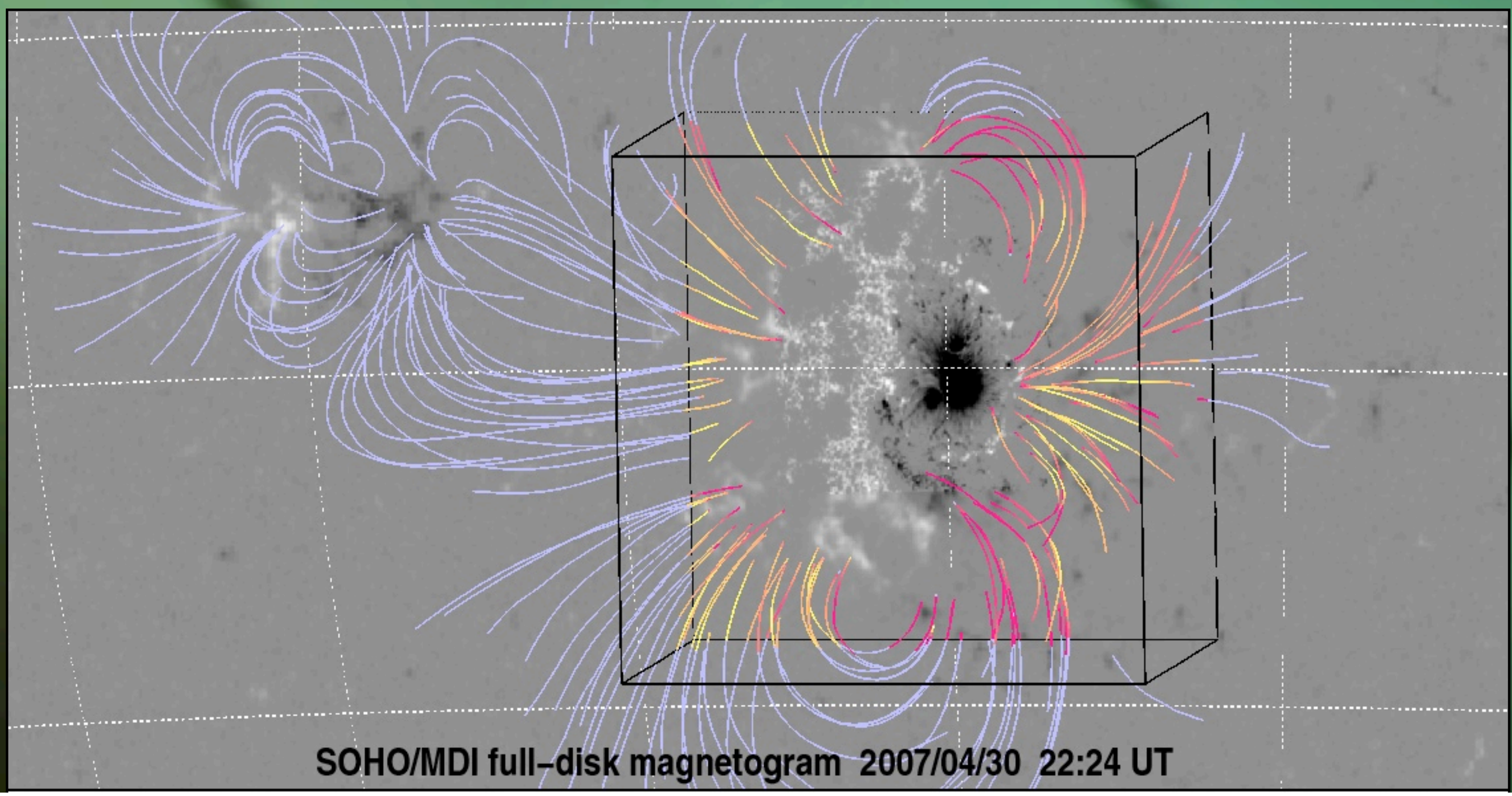

Table of metrics for AR 10953

FIELD EXTRAPOLATION METRICS[a] FOR AR 10953

Model[b]	$E/E_{\rm pot}$ [c]	$\langle \text{CW} \sin\theta \rangle$ [d]	$\langle \lvert f_i \rvert \rangle$ [e] $(\times 10^8)$	$\langle \phi \rangle$ [f]
Wh^-	1.18	0.16	1.9	27°
McT	1.15	0.37	15.	38°
Val	1.12	0.19	99.	59°
Wie	1.08	0.46	20.	32°
Tha	1.04	0.52	34.	25°
Wh^+	1.03	0.24	7.4	24°
Rég	0.85	0.42	6.3	44°
Pot	1.00	—	0.02	24°

Table of metrics for AR 10953

FIELD EXTRAPOLATION METRICS[a] FOR AR 10953

Model[b]	E/E_{pot} [c]	$\langle \mathrm{CW} \sin\theta \rangle$[d]	$\langle \lvert f_i \rvert \rangle$[e] ($\times 10^8$)	$\langle \phi \rangle$[f]
Wh^-	1.18	0.16	1.9	27°
McT	1.15	0.37	15.	38°
Val	1.12	0.19	99.	59°
Wie	1.08	0.46	20.	32°
Tha	1.04	0.52	34.	25°
Wh^+	1.03	0.24	7.4	24°
Rég	0.85	0.42	6.3	44°
Pot	1.00	—	0.02	24°

What is going on?

- Photosphere has Lorentz and buoyancy forces.
  - Data inconsistent with model assumption.
  - Codes have trouble converging/optimizing when applied to forced boundary data.
  - Codes did perform well when applied to force-free cases with known solutions.
- Preprocessing is an attempt to mitigate this.
  - Boundary data altered to reduce net forces and torques.
  - Laplacian smoothing also applied.
  - Results are better with preprocessing than without.

Conclusions

- NLFFF models should not inherently be trusted.
- A more physically realistic method is needed to capture the photosphere-to-corona interface to better transform the forced photospheric boundary data to (an approximation of) the force-free field in the low corona.
- Smaller problems:
  - Fields of view often too small (not all currents captured, edge effects cause issues).
  - Codes need some way to take into account uncertainties in the boundary data.